DEVELOPMENT AND NUMERICAL SIMULATION OF ULTRA-OPEN MULTI-DRIVER HEADPHONES FOR INDIVIDUALIZED BINAURAL REPRODUCTION

Benjamin Pries[1], Stephan Preihs[1], Jürgen Peissig[1]

[1] *Institut für Kommunikationstechnik, Leibniz Universität Hannover, Germany*

Abstract

Current headphone-based binaural audio playback systems rely on stereo headphones. Their frequency response, shaped by interactions between the sound field produced by the transducer, the headphone cup, and the pinna, is typically equalized first to enable hardware-independent playback. Individual adaptation to the user is then achieved using direction-dependent head-related transfer functions. In contrast, this paper presents multi-driver headphones featuring a total number of 30 dynamic micro-speakers, along with an associated simulation model, with which a fundamentally different approach can be pursued: The ultra-open design minimizes structural influence on the generated sound field, so transfer functions are primarily influenced by the enclosed pinna. The large number of transducers enables excitation of individual, direction-dependent pinna cues that may be used to customize the auditory impression. The numerical simulation model provides highly precise sound field data for developing advanced signal processing under ideal, disturbance-free conditions, while the physical headphones enable subsequent metrological and psychoacoustic evaluation. Design and manufacturing aspects are discussed, and the simulation model is validated in the frequency domain using measurements of sound pressure and particle velocity. Measured and simulated data show good agreement across the investigated frequency range.

Keywords: *Multi-Driver Headphones, Numerical Simulation, Prototype*

1. Introduction

The idea of using so-called multi-driver headphones with more than one transducer per ear for enhanced reproduction of binaural audio is not new. Since more than 25 years, publications deal with hardware realizations of multi-driver headphones and corresponding signal processing strategies to excite individual pinna cues. Even though setting up multi-driver headphone prototypes typically involves large constructional challenges, original designs utilizing electrodynamic transducers [1], or micro-electro-mechanical system (MEMS) speakers [2], [3], as well as modifications of existing headphones by equipping them with additional speakers [4] can be found in the literature. While MEMS speakers may become the transducers of choice in the future, small electrodynamic transducers currently still outperform them in terms of reproducible audio bandwidth and overall sound fidelity, especially for ultra-open circumaural headphone applications. Therefore, the prototype developed in this paper relies on electrodynamic transducers.

Publications focusing the required signal processing for multi-driver headphones are often based on numerical simulations that apply various simplifications like utilizing ideal monopole point sources without incorporating any near-field effects and neglecting the geometry of the headphone cup and its potential influence on the reproduced sound field [5]–[7]. Although these simplifications are reasonable for demonstrating the basic functionality of the algorithms, performance in real-world applications would benefit significantly from the utilization of a realistic simulation model of the transducers and the headphone cup already in the development process. To the best knowledge of the authors, such a combination of a physical multi-driver headphone prototype and a matching virtual prototype has not yet been used or published.

Recent advancements in rapid prototyping, especially evolving 3D-printing technology, and the increasing availability of computational power for complex numerical simulations have made the development and implementation of advanced research platforms more accessible than ever. The multi-driver headphone

Corresponding author: *benjamin.pries@ikt.uni-hannover.de.*

prototype and its corresponding simulation model provided in this paper enable detailed, non-invasive analysis of the sound fields created by each transducer and allows seamless transferability of algorithms developed later to the hardware platform.

2. Headphone Prototype

The developed multi-driver headphone prototype is shown in Fig. 1. In the following, its characteristics are presented and a detailed explanation of the design process is provided.

Each cup consists of 15 electrodynamic transducers with a diameter of 12 mm, which are arranged on a hemispherical surface with a radius of 45 mm, with their axes oriented radially toward the center of the hemisphere. By positioning the transducers as listed in Tab. 1, a balanced transducer distribution across the headphone cup is achieved while also accounting for the higher localization resolution of humans in azimuthal direction compared to the elevation direction [8]. Transducer positions are specified in the headphone cup-related coordinates φ' and θ'. Azimuth angles of $\varphi' = 0°$ and $\varphi' = 180°$ at $\theta' = 0°$ elevation correspond to positions in front of and behind the pinna, and elevation angles of $\theta' = \pm 90°$ refer to positions above and below the pinna. Even though this configuration is not yet optimized for later introduced signal processing algorithms, it already serves as a reasonable starting point for first investigations. The design steps described below can be applied to any future transducer configuration.

Table 1: Transducer positions in the left headphone cup.

Azimuth φ' [deg]	Elevation θ' [deg]
0, 30, 60, 90, 120, 150, 180	0
30, 90, 150	±45
n.a.	±90

Ole Wolff OWR 1228T-32B transducers are selected for the prototype. In general, transducers developed for active noise control applications are suitable here as their capability of producing large excursion at low frequencies also enhances low-frequency output, which is typically considered as a major challenge in ultra-open headphones. Furthermore, it is noted that a gain of up to 23.5 dB can by achieved by operating all transducers in phase compared to a single transducer, providing sufficient headroom for broadband audio playback.

For easy replacement of individual transducers in the case of a defect, the transducers are not installed directly into the cups but are clipped into the cups using mounting rings. A cross-sectional view is provided in Fig. 2. While the inner part of the mounting ring is made of polylactide (PLA), the outer part serves as a flexible sealing ring made of thermoplastic polyurethane (TPU) providing tight fit and dampening mechanical vibrations to minimize the excitation of the modal frequencies of the cup.

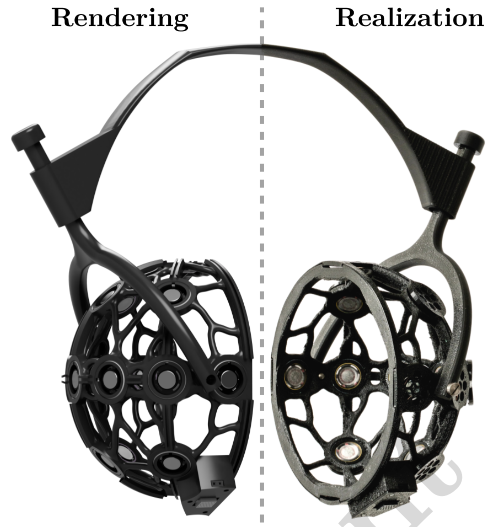

Figure 1: Multi-driver headphones. Left side: Rendering of the 3D CAD model. Right side: Photo of the prototype.

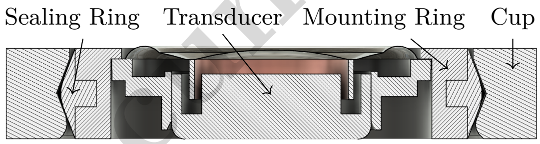

Figure 2: Cross-sectional view of the clip-in mechanism for mounting transducers in the cup.

Furthermore, a modified version of the headband of the so-called *Mushroom Headphones* [9] is employed. The cups and the headband are made of 3D-printed carbon-fiber-reinforced polyamide, which ensures high stiffness and high temperature resistance. To prevent cables from being touched and potentially damaged while handling the prototype, a flexible TPU cover is stretched over the outer surface of the cups.

2.1. Generative Design Approach

During the development process, initial prototypes with manually designed mechanical links between the transducers forming the cup exhibit significant artifacts in the measured frequency responses. This was attributed in particular to insufficient stiffness of the cup. Therefore, inspired by the Mushroom Headphones [9], a bionic design approach utilizing Autodesk Fusion 360's generative design feature is followed to increase the stiffness while maintaining an ultra-open design.

The hollow cylinders into which the transducer mounting rings will be inserted, the attachment points for the headband, and a base ring that serves as the contact surface at the head are specified as preserve geometries (Figure 3a). The design space is limited inside the transducer array by a hemisphere with a radius of 44 mm and by a plane parallel to the base ring. Furthermore, areas for transducer and headband attachment are excluded from the design space (Figure 3b).

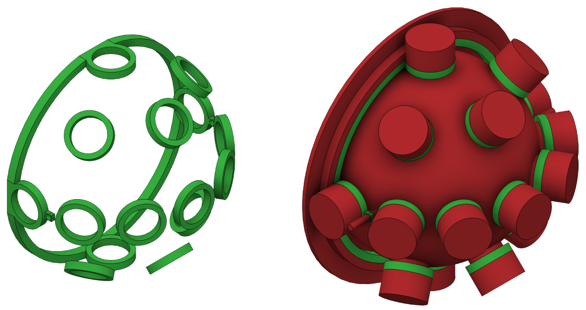

(a) **(b)**

Figure 3: Design space for generative headphone cup design: (a) Preserve geometries. (b) Obstacle geometries.

Since Fusion 360 supports only static forces and moments, harmonic loads generated by transducer vibration cannot be directly incorporated into the design study. These loads are too small to have any significant influence on the results of the design study compared to, for example, the headband clamping force anyhow. Instead, multiple load cases are defined, whose magnitudes rather represent loads that might occur while handling the cup, while at the same time being applied at the transducer positions. Radial forces (1 N on each ring), moments (4.5 N mm) in the azimuth direction and in the elevation direction are considered. In addition to load cases in which the load is applied in the same direction at each transducer position, asymmetric cases are also defined in which the loads on adjacent positions are applied in opposite directions. Furthermore, a headband clamping force of 4 N at the attachment points and a corresponding reaction force on the base ring are taken into account. While pin constraints are applied at the headband attachment points, the rotation around the axis through these points is not constrained. Instead, the *Remove rigid body modes* feature is enabled in the design study settings. The goal of the design study is set to *maximize stiffness* and a mass target of 20 g is selected. Carbon-fiber-reinforced polyamide (PA603-CF) is used as the study material.

2.2. Design Refinements and Analysis

In the final design, cable channels and a mounting option for a small printed circuit board (PCB), which allows the use of a detachable cable, are manually integrated.
Modal analysis of the cup reveals a reduction of 38% in the number of possible vibration modes at frequencies below 4 kHz compared to a manually designed cup (53% below 2 kHz). Even though isotropic material properties are assumed in this analysis, which does not hold for 3D-printed parts manufactured using fused deposition modeling (FDM), and therefore does not allow direct transfer of the results to the manufactured cup, the designed cup exhibits significantly improved stiffness while maintaining its acoustical openness.

3. Simulation Model

The simulation model of the multi-driver headphone prototype is implemented in COMSOL Multiphysics. It is presented in two parts below: First, the modeling of the transducers is outlined, followed by explanations on the virtual prototype setup and the applied simplifications for achieving a reasonable model complexity and simulation run time.

3.1. Transducer Simulation

A hybrid approach similar to the one described by Marttila and Jensen [10] is utilized for the numerical simulation of the transducer with some modifications: The electro-mechanical properties of the transducer are represented through a lumped-element circuit model (Fig. 4) which is bidirectionally coupled to the finite element acoustics simulation via the equivalent radiation area of the diaphragm of the transducer. This is achieved in COMSOL by applying the *Interior Lumped Speaker Boundary*. In the equivalent circuit diagram, this is represented by the voltage source F_d. To avoid the requirement of further knowledge on material properties of the diaphragm, only rigid motion of the equivalent radiation area of the diaphragm is simulated instead of using shell elements. This simplification, also introduced in [11], works particularly well for very small micro-speakers with stiff diaphragms as partial vibration modes due to cone breakup typically appear only at very high frequencies.

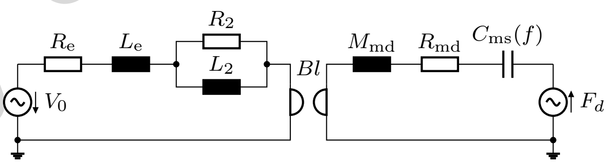

Figure 4: Lumped element circuit of the electrodynamic transducer.

The small signal parameters of the transducer listed in Tab. 2 were determined in vacuum using a Klippel Analyzer System. Minor parameter tuning was performed for best fit of the simulated and measured electrical impedance and diaphragm excursion. For the equivalent radiation area S_d, the differential measurement technique described in [12] was utilized. The creep effect of the suspension at low frequencies is taken into account by using a frequency dependent compliance model [13]

$$C_{ms}(f) = C_{ms} \cdot \left(1 - \lambda \cdot \log_{10}\left(\frac{f}{f_0}\right)\right) \qquad (1)$$

with the resonance frequency $f_0 = 266.8$ Hz, the compliance $C_{ms} = 11.231$ mm/N at f_0 and the creep factor $\lambda = 0.25$.

For the acoustics domain, a fully three-dimensional geometry representation of the transducer is set up based on the outer dimensions provided by the manufacturer and further measurements of the inner geometry. A cross-sectional view of the geometry is

Table 2: Small signal parameters of OWR 1228T-32C.

Category	Parameter	Value
Electrical	R_e	31.17 Ω
	L_e	0.125 mH
	R_2	1.31 Ω
	L_2	0.017 mH
Electromech. Coupling	Bl	0.855 N/A
Mechanical	M_{md}	0.032 g
	R_{md}	0.016 kg/s
	C_{ms}	11.231 mm/N
Geometric	S_d	78.54 mm^2

provided as part of Fig. 2. Losses in the rear vents of the transducer as well as in the air gaps of the magnetic circuit around the voice coil are taken into account using the *Narrow Region Acoustics* model in COMSOL. The damping mesh which is glued to the rear vents of the transducer is incorporated in the simulation model as an interior impedance condition. Its transfer impedance is determined in a separate simulation study similar to the procedure described in [14]. First, the mesh was examined under a microscope, followed by a parameter sweep over reasonable hole sizes and thicknesses of the mesh, while keeping the hole-to-hole spacing constant. The obtained transfer impedances were then tested in the transducer simulation model and the parameter combination that best replicated the experimentally determined differences in electrical impedance and diaphragm excursion with and without the damping mesh was selected. Additional minor losses are accounted for by applying a real valued frequency-independent boundary impedance of $Z = 100\rho_0 c$ (ρ_0: density of air, c: speed of sound) to all internal walls of the transducer.

In Fig. 5 and 6, the measured electrical impedance and diaphragm excursion are displayed in comparison with the simulation results, with and without the damping mesh on the rear openings, respectively. The excellent agreement across the entire frequency range demonstrates that the electromechanical properties of the transducer are correctly captured in the simulation model. This is further confirmed by the on-axis free space sound pressure level measurement displayed in Fig. 7, revealing a deviation of less than 2 dB for frequencies above 200 Hz with an average absolute deviation of 0.8 dB. The minor discrepancy in the low-frequency roll-off is attributed to a significant temperature dependence of the mechanical compliance C_{ms}, observed during our investigations, leading to variations of the resonance frequency of the transducer.

3.2. Virtual Prototype

For the virtual prototype, small details of the headphone cup such as the cable channels and the PCB mounting box, as well as the mechanisms for installing the transducers into the cup, are omitted. A boundary impedance of $Z = 100\rho_0 c$ is applied to all 3D-printed parts.

In addition, a passive transducer dummy is introduced whose external geometry matches that of the complete transducer model, but which does not include the internal details. It can be employed as a placeholder to avoid having to simulate 15 complete transducer models, even in cases where only the sound field of a single transducer is examined, without neglecting the feedback effects of the other passive transducers on the sound field. To determine the passive impedance by assessing sound pressure and particle velocity at the diaphragm, the complete transducer model was positioned in an external plane wave sound field without supplying any input voltage to the transducer terminals. The obtained impedance is then applied to the diaphragm boundary of the dummy.

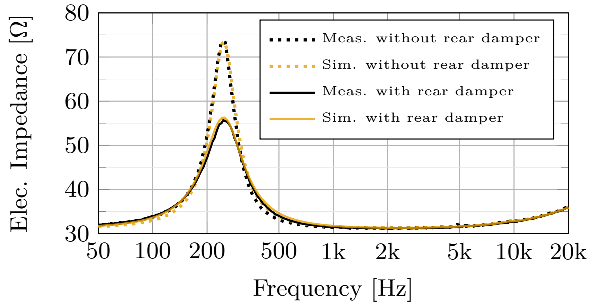

Figure 5: Magnitude of the electrical impedance.

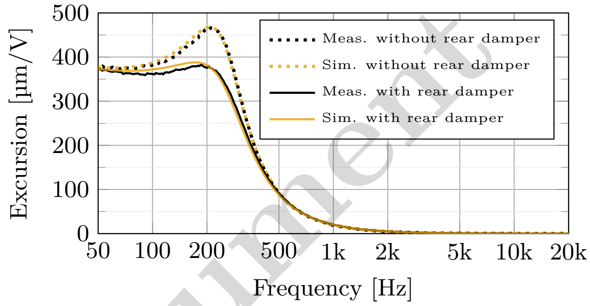

Figure 6: Diaphragm excursion transfer function.

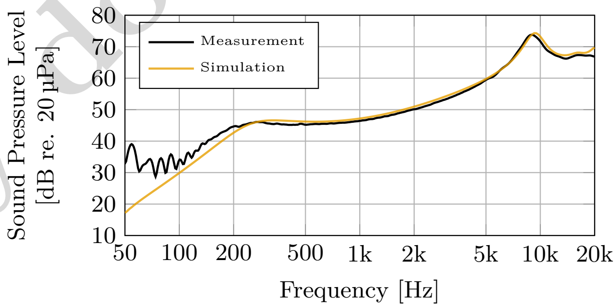

Figure 7: On-axis sound pressure level in a distance of 5 cm for an input voltage of 200 mV$_{rms}$.

4. Validation

To validate the virtual prototype, sound pressure and particle velocity measurements were conducted with the headphone cup mounted on a flat rigid plate. Measurements were acquired at the center of the cup and at five additional locations positioned ± 25 mm from the center along the axes of the headphone cup-centered cartesian coordinate system. A one-dimensional sound intensity probe (Microflown PU Match) was employed for all measurements. By rotating the probe 90 degrees around its axis, the particle velocity was captured in two directions. All measurements are smoothed using a 1/24-octave smoothing procedure first and subsequently interpolated to the simulation frequencies to enable comparison. To avoid that positioning errors of the probe during the measurement lead to an overestimation of the simulation error, an uncertainty range is introduced. Therefore, the sound pressure and particle velocity are evaluated in the simulation not only at the point where the probe is expected, but also at 6 additional points, each shifted by ± 2 mm along each coordinate axis. The maximum and minimum values determined at these points define the uncertainty range. If a measured value falls within these limits, a deviation of 0 is assumed. Examples of the measured sound pressure level and particle velocity and the corresponding simulation results are shown in Fig. 8 and 9.

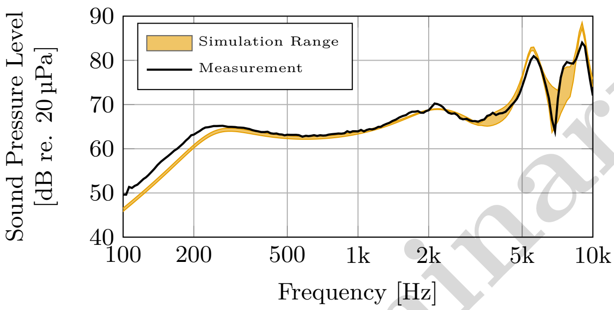

Figure 8: Exemplary measured sound pressure level and simulation range for positional uncertainty of the measurement probe at the center of the cup for a transducer positioned at $\varphi' = 30°$, $\theta' = 45°$.

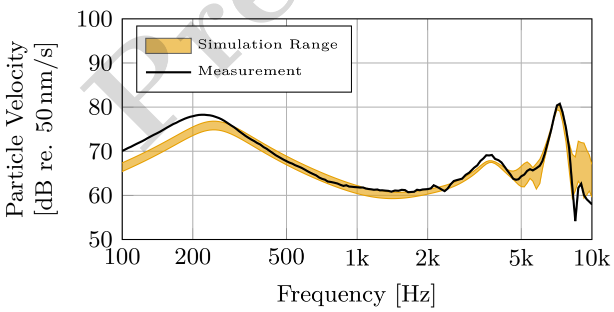

Figure 9: Exemplary measured particle velocity in x-direction and simulation range for positional uncertainty of the measurement probe at the center of the cup for a transducer positioned at $\varphi' = 30°$, $\theta' = 45°$.

The resulting absolute deviations between the simulation and the measurements across all measurement positions are shown in Fig. 10 for the sound pressure, and in Fig. 11 for the particle velocity respectively. In Fig. 11, the combined results for the x- and z-component of the particle velocity are shown, whereby only measurements are considered in which the angle between the line connecting the transducer and the measurement position, and the sound velocity sensor orientation does not exceed 75 degrees. As the upper limit of the operating range of the measurement probe is specified to be 10 kHz, results are only shown up to this frequency.

Overall, there is good agreement between the simulation and the measurement results for both, sound pressure and particle velocity. Across a broad frequency range, the median reveals no or only minor deviations from the defined uncertainty range. In general, a slightly larger deviation is observed for the particle velocity than for the sound pressure. Nevertheless, above 200 Hz, the average of the 90th percentile of the absolute magnitude deviation is only 1.8 dB for the particle velocity compared to 0.8 dB for the sound pressure. As already discussed for the transducer simulation model, the shift in the low frequency roll-off due to the temperature dependent mechanical compliance also applies here, leading to deviations in magnitude and phase of both, sound pressure and particle velocity. Increasing deviations at high frequencies are attributed to the growing influence of the measurement probe on the sound field. Furthermore, temperature differences also impact the speed of sound in air, contributing to increasing phase deviation towards high frequencies.

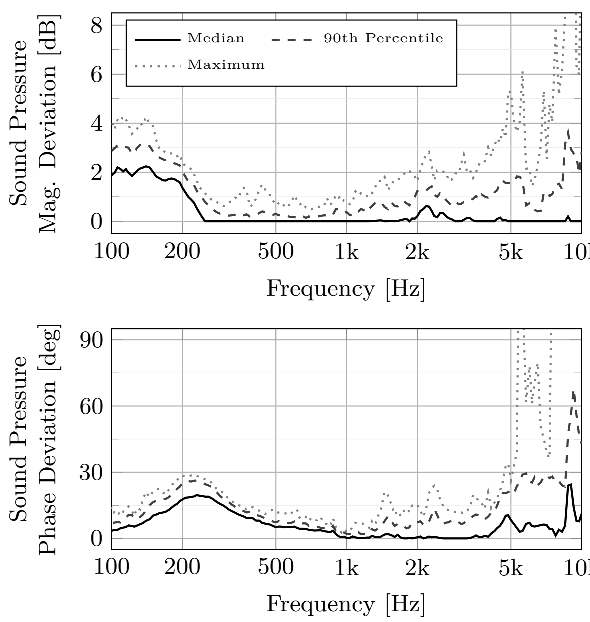

Figure 10: Magnitude and phase deviation of the sound pressure between measurement and simulation that exceeds the variation caused by positioning uncertainty.

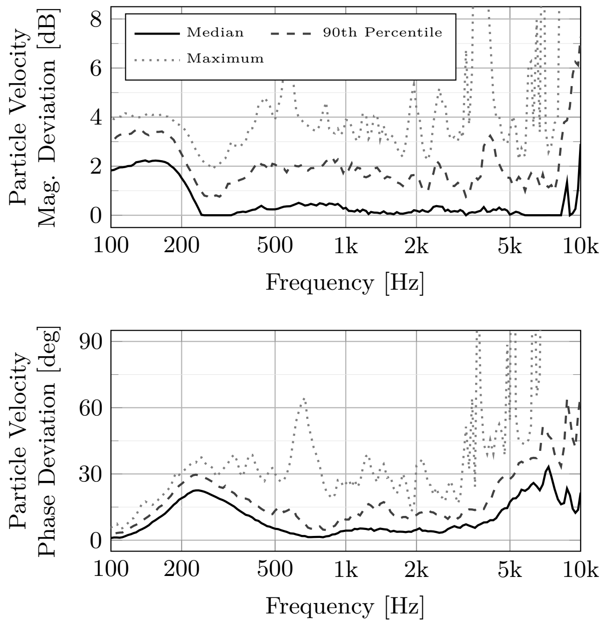

Figure 11: Magnitude and phase deviation of the particle velocity between measurement and simulation that exceeds the variation caused by positioning uncertainty.

5. Conclusion

The development process of a mechanically optimized multi-driver headphone prototype, and an associated virtual prototype were presented. The simulation model was validated using measurements of sound pressure and sound velocity at several positions within the headphone cup. The resulting deviations are within the usual tolerance ranges and can be explained by temperature effects as well as by underlying differences between the measurement setup and the simulation, in particular the absence of the measurement probe in the simulation. Thus, the suitability of the simulation model for capturing sound field data for the development of advanced signal processing algorithms for personalized binaural playback is confirmed.

6. Supplementary Material

All parts for 3D-printing the presented multi-driver headphone prototype are publicly available online: `https://gitlab.uni-hannover.de/scrudriva/multi-driver-headphones`.
Additional files related to the designed circuit boards can be provided upon request.

7. Funding

This work was funded by the Deutsche Forschungsgemeinschaft (DFG, German Research Foundation) – project number 562226092.

References

[1] R. Greff, "Holophonie binaurale - spatialisation sonore sur réseaux de haut-parleurs circumauraux," Ph.D. dissertation, Universite Paris VI, Paris, France, 2008.

[2] A. Vilkaitis and M. Lucchi, "Development and analysis of a MEMS based multi-driver headphone to introduce individualised pinnae frequency shaping," presented at the AES 148th Convention, 2020.

[3] A. Neacsu, M. Lucchi, F. Pausch, P. Majdak, and T. Amann, *Selfone (tool #7)*, 2025. DOI: 10.60887/wkrqcfmma4qpyczr.

[4] H. Pomberger, A. Sontacchi, M. Frank, T. Gmeiner, and M. Lucchi, "Improved localization in the median plane with cue-preserving headphones," in *Fortschritte der Akustik - DAGA 2018*, 2018, pp. 948–951.

[5] I. Chun and P. A. Nelson, "Virtual acoustic system with a multichannel headphone," presented at the AES 115th Convention, 2003.

[6] J. Wang, P. Samarasinghe, T. Abhayapala, and J. A. Zhang, "Binaural reproduction using multi-driver headphones," presented at the 2022 Int. Workshop on Acoustic Signal Enhancement (IWAENC), 2022. DOI: 10.1109/IWAENC53105.2022.9914750.

[7] B. Pries, S. Preihs, and J. Peissig, "Towards the practical feasibility of head-related sound field synthesis using multi-driver headphones," presented at the AES Int. Conference on Headphone Technology, 2025.

[8] J. Blauert, *Spatial Hearing: The Psychophysics of Human Sound Localization.* The MIT Press, 1996, ISBN: 978-0-262-26868-4. DOI: 10.7551/mitpress/6391.001.0001.

[9] A. Mülleder and F. Zotter, "Ultralight circumaural open headphones," presented at the AES 154th Convention, 2023.

[10] P. Marttila and M. J. H. Jensen, "A hybrid electroacoustic lumped and finite element model for modeling loudspeaker drivers," presented at the AES Conference: 51st Int. Conference: Loudspeakers and Headphones, 2013.

[11] COMSOL Multiphysics, *Lumped loudspeaker driver*, 2015. [Online]. Available: https://www.comsol.com/model/lumped-loudspeaker-driver-12295 (visited on 07/22/2026).

[12] Klippel, *AN 32: Effective radiation area S_d*. [Online]. Available: https://www.klippel.de/fileadmin/klippel/Files/Know_How/Application_Notes/AN_32_Effective_Radiation_Area.pdf (visited on 09/24/2024).

[13] M. Knudsen and J. G. Jensen, "Low-frequency loudspeaker models that include suspension creep," *Journal of the AES*, pp. 3–18, 1993, ISSN: 1549-4950.

[14] COMSOL Multiphysics, *Transfer impedance of a perforate*, 2016. [Online]. Available: https://www.comsol.com/model/transfer-impedance-of-a-perforate-12585 (visited on 11/14/2025).